Date of publication xxxx 00, 0000, date of current version xxxx 00, 0000.

Digital Object Identifier 10.1109/ACCESS.2025.0000000

Integrated multi-converter maximum power point tracker for direct-drive of variable loads demonstrated with electrodialysis desalination

JONATHAN T.-Y. BESSETTE[1], (Member, IEEE), SHANE R. PRATT[1], and AMOS G. WINTER, V.[1]

[1]Department of Mechanical Engineering, Massachusetts Institute of Technology, Cambridge, MA 02139 USA (e-mail: jbessett@mit.edu)

Corresponding author: Jonathan T.-Y. Bessette (e-mail: jbessett@mit.edu).

This work was supported by the National Science Foundation Graduate Research Fellowship under grant number 1745302, the Julia Burke Foundation, the Abdul Latif Jameel Water and Food Systems Lab (J-WAFS) Rasikbhai L. Meswani Fellowship for Water Solutions, and the K. Lisa Yang Global Engineering & Research Center.

ABSTRACT Typical maximum power point trackers (MPPT) in off-grid applications use one power converter (e.g., a buck-boost) to draw the maximum power from a solar array by algorithmically altering the duty cycle to charge a battery, which then supplies power to multiple downstream loads. However, some applications could have multiple loads directly-driven by the photovoltaic array, rather than buffered by a battery or other energy storage, if these loads are able to operate at variable power. This work demonstrates a control architecture that enables simultaneous MPPT and load regulation using only downstream converters, eliminating the need for both energy storage and a centralized MPPT converter. We take a canonical MPPT method and weight its output command uniquely for each individual converter, based on each individual converter's objective. This allows us to simultaneously optimize power allocation to the variable loads, while tracking the maximum power point. The approach was demonstrated using an electrodialysis (ED) desalination system as the source of two variable loads: the pump and ED stack. We demonstrate power tracking within $14.3 \pm 2.3\%$ of the maximum power point throughout the experiment amidst step responses to the maximum power point while simultaneously maintaining desalination operation within $10.3 \pm 0.3\%$ of the optimum setpoint. Integrating MPPTs with downstream converters can eliminate an entire power converter and energy storage system, reducing cost and increasing overall efficiency.

INDEX TERMS Maximum Power Point Tracking (MPPT), Multi-converter, Desalination, Electrodialysis, Photovoltaic (PV), Cascaded Feedback Control.

I. INTRODUCTION

SOLAR photovoltaic (PV) energy is projected to grow from 3% of the United States' energy supply to 45% by 2050 and is the renewable energy technology with the highest growth rate [1]. However, solar photovoltaic panels pose the challenge of intermittent energy supply. These intermittencies cause problems for loads which typically run at constant power. They also create challenges in extracting the maximum available power from the solar panels; as the solar irradiance fluctuates, the maximum available power changes.

A maximum power point tracker (MPPT) is a controller designed to continuously draw maximum power from a photovoltaic (PV) panel, despite intermittencies caused by fluctuations in solar irradiance, temperature, array configuration, and other factors. MPPTs address the challenge of PV panels' current-voltage (IV) curves, which are affected by environmental and system conditions—such as temperature, shading, and soiling—that alter the available maximum power point. These controllers typically operate with a single DC/DC converter (Fig. 1A) and adjust the duty cycle to optimize the voltage and current drawn from the panel. Simple MPPT algorithms such as fractional open circuit voltage (FOCV) and perturb and observe (P&O) are widely used for their robustness and ease of implementation, though they are limited in more complex scenarios [2]. More advanced MPPT algorithms incorporate measurements of irradiance, temperature, and weather predictions, offering greater precision but increased complexity [3].

A. A MULTI-CONVERTER MPPT AND ITS CHALLENGES

Few MPPT algorithms consider multiple converters downstream of the solar panel (rather than just one converter,

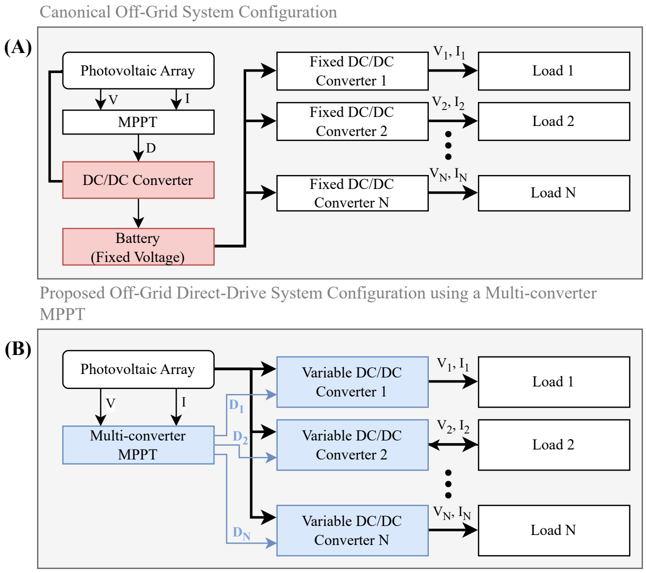

FIGURE 1. (A) A general MPPT architecture for an off-grid PV system with a battery. Downstream loads operate from converters with relatively fixed input and output voltages sourced by the constant battery voltage. (B) Proposed multiload MPPT architecture, where the duty commands to the DC/DC converters are sourced directly from a supervisory controller and the power sources for these converters are directly from the photovoltaic array. Note that in this architecture, both the battery and DC/DC converter associated with canonical configuration are no longer necessary, potentially reducing cost and increasing efficiency.

e.g., Fig. 1B). This is due to solar arrays most commonly being installed with a battery bank or a grid connection. Most loads operate at nominal, constant power and are not designed to handle intermittencies; purely off-grid systems thus rely on energy storage to act as a buffer and provide a consistent source. However, there exist loads which can operate at variable power and thus can operate in direct-drive configuration: directly coupled solar to load with no energy storage in between (e.g., no batteries). There are many commercial examples of direct-drive MPPT algorithms for single converters coupled with a single load, such as a solar refrigerator or a solar powered pump (where the MPPT power converter is often called a solar pump inverter [4], [5]). However, none, to the authors knowledge, exist for multiple direct-drive (batteryless) loads in an off-grid setting (as proposed in Figure 4).

The design of multiport converters with integrated MPPTs are related to this problem. However, most work focuses on balancing the combination of several input power sources such as solar, wind, and grid [6]–[8], rather than optimally regulating a multiple load output. Some authors have explored multiload control but utilize battery storage or grid inputs [9] and often in simulation rather than in practice.

Some examples of a potential multi-load system include a single MPPT designed to directly allocate power to two different DC freezers, each with its own temperature setpoint. Another example could include two solar-powered pumps in a chemical process, one of which must always operate at half of the flow rate as the other. A final example includes direct-drive of several electrolyzers from solar power [10]. In this example, the MPPT algorithm and converter are independent of the downstream electrolyzer load converters.

The creation of a multiple load, direct-drive MPPT has several benefits. Firstly, this architecture would eliminate at least one power converter, which would increase the energy efficiency and decrease the overall cost of the system. Secondly, the direct-drive operation of several converters in cooperation eliminates the need for intermediate energy storage (i.e., batteries); whereas off-grid PV systems with more than one load traditionally require energy storage. Batteries can increase the capital and operating cost and could have detrimental beginning and end-of-life environmental affects.

However, a multiple load, direct-drive MPPT has several challenges. Firstly, it is nontrivial to simultaneously satisfy both tracking the maximum power point, while optimally distributing the extracted solar power to multiple loads. This is especially true when the loads have varying ranges of operating power bandwidth, responsiveness, operating requirements, and optimal setpoints. In addition, there are cases where the power output to one of the loads may affect the optimal set point of another load. All of these complications are necessary to consider when designing an integrated, multi-converter MPPT. In this work, we explore the design of such a converter for an electrodialysis desalination system, which has two loads which may operate with variable power: the electrodialysis stack and the pump.

B. A MULTILOAD, DIRECT-DRIVE-CAPABLE SYSTEM: ELECTRODIALYSIS

Electrodialysis (ED) is an electrochemical separations technique (Fig. 2) used in many applications, including desalination of water and the production of acids and bases [11]. It traditionally requires at a minimum, two power converters (Fig. 3): one power supply to drive the flow of ions through the electrodialysis stack, via electrodes mounted on both ends of the stack and the second power supply to control the flow rate of water through the stack via a pump, most commonly centrifugal.

The electrodialysis stack load is analogous to a variable resistor which varies with the solution concentration. In desalination, this resistance decreases with higher salt content, and contrastingly increases with lower salt content. In other words, as the system desalinates closer to drinking water levels of salinity, the resistance increases. A voltage is applied to the electrodes from the stack (converter) power supply, driving current and the transport of salt ions through the selectively permeable ion-exchange membranes desalinating the water.

The electrodialysis stack loading is constrained to an upper bound by water dissociation, which occurs when overlimiting current is applied; operation must be below limiting current. Hydraulic loading is also restricted to an upper limit by the maximum pressure drop across the stack set by manufacturers as well as by the pump capabilities. The ability to widely

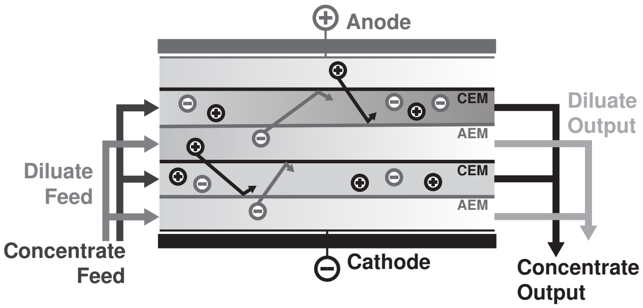

FIGURE 2. **Electrodialysis stack cross section. The stack consists of a diluate (diluted, or less concentrated) stream and concentrate stream of inlet and outlet solution. The ions within the stack pass through selectively permeable membranes based on charge, denoted as cation exchange membranes (CEM)s and anion exchange membranes (AEMs).**

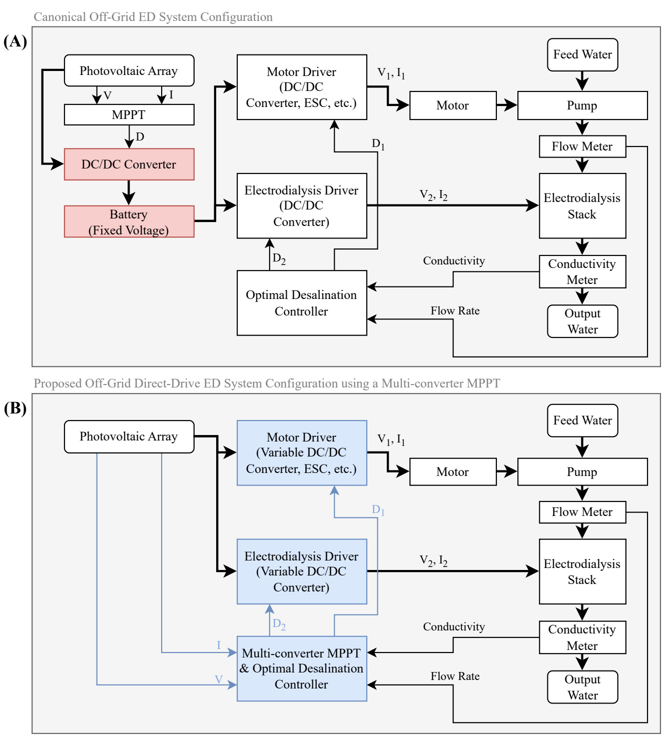

FIGURE 3. **(A) A typical, generalized photovoltaic electrodialysis system layout from prior art [12], [13]. (B) Proposed combined MPPT & optimum desalination controller in the context of a photovoltaic electrodialysis system.**

vary flow rates in the stack facilitates variations in hydraulic power, and the ability to vary stack voltage and current facilitates variations in electrodialysis stack power, thus providing two variable power loads that we may dynamically operate.

There is interest in utilizing solar energy with electrodialysis in direct-drive (batteryless) operation. Desalination without energy storage is a field of growing investigation, as the elimination or reduction of batteries lowers capital expenditure, volume, and operational complexity. However, the challenge specific to direct-drive, PV electrodialysis is optimally allocating power to the ED stack and the pump(s) to maximize water production rate, while also tracking the maximum power point.

Prior art exists which has accomplished this using feedback control [13] as well as via a predictive model [12]. However, the prior art in feedback control utilized an off-the-shelf integrated MPPT DC/DC buck converter and several DC/DC power supplies which lacked coordination and communication with one another, and had competing objectives. For instance, the off-the-shelf MPPT would trigger an MPPT search and rapidly drop the current drawn from the PV panel without warning to the downstream DC/DC supplies, which subsequently would overdraw current from the battery buffer. While this work significantly reduced the necessary energy storage size for PV-ED, a small battery was still necessary for maintenance of controls, sensing, occasional power overshoots in downstream converter responses, and to accommodate the lack of MPPT search coordination. The prior art in predictive model-based control did not consider aspects of latent power draws, computation time problems, and error accrual in their model performance due to physical degradation of the system. Hence, in the aforementioned prior art, the complete elimination of battery storage was not accomplished. Thus, this provides a good example case for us to explore the development of a multi-converter MPPT.

The aim of this work is to design and test a multi-converter, direct-drive maximum power point tracker which demonstrates simultaneous (1) optimal power distribution to the two main loads, the ED stack and pump(s), and (2) track and maintain the maximum power point. In this case, we aim to design an integrated MPPT solar pump inverter with an electrodialysis power supply for the application of direct-drive electrodialysis desalination. Accomplishing this will demonstrate that such a multi-converter MPPT system is feasible as well as eliminate battery storage and a power converter in a practical application.

II. CONTROL THEORY

A. GENERALIZED DIRECT-DRIVE MULTI-CONVERTER MPPT

For a general multiconverter MPPT, there is the overarching objective of maximizing power drawn from the solar array, and there are individual sub-objectives for each load and power converter, depending on the load requirements. To accomplish these simultaneous aims, we propose combining the MPPT controller, traditionally related to one power converter, with the downstream converter controls. A single, integrated controller reads both the status of the solar panel (e.g., current, voltage, temperature) as well as any downstream process sensor(s) for each of the loads. This single, integrated controller then allocates the correct duty cycle to each of the individual converters and their loads, to satisfy the individual load objectives while also extracting the maximum power from the solar array.

A form of this concept involving feedback control is shown in Figure 4. In Figure 4A, a scheme is proposed where the converters all receive a common commmand signal from any standard generalizable MPPT algorithm. These signals are

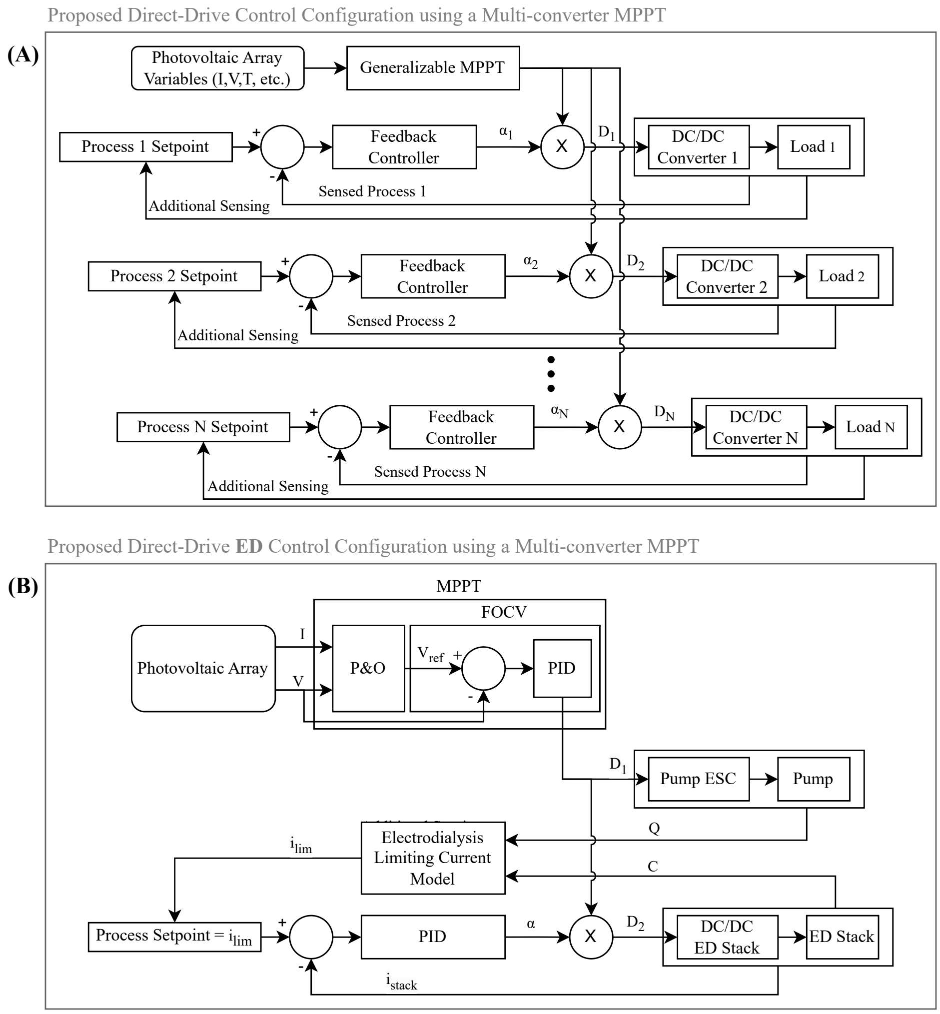

FIGURE 4. **(A) Proposed generalized multiload MPPT block diagram. (B) Electrodialysis desalination dual converter MPPT block diagram.**

then independently biased by a weighting factor, α_i for a process within the set $i = 1 : N$, where N indicates the number of processes in the system. This weighting factor varies via feedback control depending on the individual load objective and related sensing. For instance, if the load is a refrigerator that is becoming too warm, the feedback controller may increase α_i to send a greater portion of total extracted power to the refrigerator. This is just one manifestation; others may propose more complex multi-converter MPPT schemes such as model predictive control, adaptive, etc.

B. ED DIRECT-DRIVE MULTI-CONVERTER MPPT

We apply the generalized framework in Figure 4A with some minor adjustments to an ED system, detailed in Figure 4B. Here, we have our generalized P&O algorithm reading the current and voltage from the photovoltaic array, outputting a reference voltage. This operating (reference) voltage is tracked using feedback control by measuring the PV array voltage and altering an overarching (common command) output duty cycle signal, D_1. Simply, D_1 is the output from our chosen MPPT algorithm, changing based on the solar panel conditions. D_1 is fed directly to the pump power converter and thus directly increases or decreases the power consumption and flow rates. D_1 is simultaneously biased by a weighting factor, α, which alters the duty to the electrodialysis stack power converter, D_2; where, $D_2 = \alpha * D_1$. The weighting factor, α, is adjusted based on a feedback loop with the objective of commanding an electrodialysis stack current, ß$_{stack}$ that matches the limiting current, ß$_{lim}$. The limiting current is the point at which water dissociates, and is determined most frequently by using an empirical model (e.g., [11]) with model inputs that include measurements of water conductivity, C, and flow rate, Q. This is the individual, sub-objective for the electrodialysis stack converter (match limiting and commanded current, to maximize desalination throughput). The individual, sub-objective of the pump is to maximize the flow rate at any given time. Both sub-objectives are necessary for maximizing desalination and water production rate, as described further in [12], [13]. Both loads concurrently consume power, which then affects the solar array voltage and current, and thus is fed back into the MPPT algorithm. This closed-loop control scheme is computationally simple. This control theory accommodates both maximum power point tracking and operation at the optimal desalination rate.

III. METHODOLOGY

A. PROTOTYPE BOARD DESIGN REQUIREMENTS

The authors had prior experience in constructing and testing home-scale (conveniently laboratory-scale) brackish water electrodialysis systems [14]–[17]; we thus chose to derive the power electronics requirements and demonstrate the proposed control scheme on a home-scale electrodialysis system. Brackish waters are often $<$ 2000 mg/L for home-scale applications and prevalent in areas from India to the American Southwest. To give a sense of size scale, systems for this application commonly are packaged in compact cabinets that are wall-mounted or installed underneath kitchen sinks. Electrodialysis stacks in this application are relatively small, approximately the size of a lunchbox, and the pumps utilized are also relatively small, positive-displacement pumps similar to those utilized in home aquariums and home garden water features.

	Stack	Pump	Control
Input Voltage (VDC)	0-60	0-60	0-60
Output Voltage (VDC)	0-24	0-24	5, 12
Output Voltage Ripple (VDC)	[-]	0.1	[-]
Input Current (A)	0-5	0-5	0-5
Output Current (A)	0-2	0-2	0.5
Output Current Ripple (mA)	6	[-]	[-]

TABLE 1. Experimental converter design requirements as values and ranges based on the usage of a home-scale electrodialysis stack (PC Cell Gmbh) and pumps (Singflo 2401). Ripple is defined from peak-to-peak.

For a home-scale electrodialysis stack operating under brackish water conditions, the typical voltages and currents applied can be up to 24 VDC and 1 A, but generally are on the order of 0.1 A. This stack size requires pumps sized in the range of 12-24 VDC and 1-2 A. Most commercially available pumps for point-of-use water treatment are in the 12 or 24 VDC category.

An important requirement is the current ripple on the electrodialysis stack. If the target current is exceeded beyond the safety factor applied, overlimiting current may be reached and water will dissociate, generating hydrogen and chlorine gas. For this system, the limiting current commands were in the range of up to 2 A. With a factor of safety of 70%, leaving 0.6 A of buffer. However, the commands can be as low as 10 mA, leaving 3 mA of buffer in the most conservative case. While it is desirable not to exceed limiting current, brief transient overshoots can be acceptable and are even periodically done to swing the pH of the system and self-clean. Thus, an ideal peak-to-peak current ripple for this system was decidedly less than or equal to 6 mA. These stacks commonly range on the order of tens to hundreds of ohms, depending on the salinity, the number of spacer and membrane pairs within it, and the electrodes.

The pumps have relatively more leniency in their fluctuations; however, excessive voltage ripple can cause flow rate fluctuations and lead to instabilities within the current control and concentration output from the stack. In this regard, we heuristically specified a voltage ripple of 100 mV.

Finally, the system was designed to accommodate a typical 100 W solar panel. Most 100 W solar panels have approximately 24 VDC open circuit voltage, and around 5 A of short circuit current. Thus, we expected our system to operate in voltages up to 24 VDC, however, we sized the system to be rated to higher voltages in case we used larger arrays with several panels in series. The design was sufficiently rated for the current output off a single panel, and we did not intend to utilize parallel strings for this home-scale application.

The full list of design requirements can be found in Table 1.

B. POWER ELECTRONICS HARDWARE

1) Converter, Switch, & Driver Choice

Multiple converters were considered, including buck-boost, flyback, and fly-buck; galvanitcally isolated DC/DC converters can be advantageous for safety in industrial-scale, high voltage electrodialysis applications, where there can be water leakage and thus operator shock risk. However, in this case, we required low voltages relative to industrial process stacks, which operate on the order of hundreds of volts. We consequently implemented a simple architecture (Fig. 5) of two, parallel buck converters: one for the stack power supply and one for the hydraulic load (two pumps). One of the pumps feeds the bulk fluid through the diluate and concentrate channels at equivalent flow rates (50% recovery ratio), and the other pump feeds an electrode rinse channel, which clears any gaseous formations from faradaic reactions. These two pumps were equivalent in the design of this experiment, and ran on the voltage bus from the pump(s) buck converter. For visual context, Fig. 6 details the laboratory-scale electrodialysis system used in this study, described further in subsection D.

We chose to design and operate a two N-channel MOSFET (Texas Instruments CSD19535KTTT) synchronous buck converter for higher power efficiency, despite the added complexity of preventing shoot-through via dead time (delay). For ease of design, we designed one buck converter to be replicated for both the stack power supply and the pump power supply. In total, we incorporated four equivalent buck converters on the board for redundancy, though only two were used in experimentation. The buck was designed to operate in continuous conduction mode (CCM), and thus, we imposed the constraint that the required current ripple must be less than or equal to the mean of the minimum inductor current, as seen in Equation 1.

The driver chosen (Texas Instruments UCC27282QDRQ1) was manufactured for a high-side, low-side configuration allowing us to use a single chip for both MOSFETs. The boostrap capacitor (0.22 μF) and surrounding passives were designed using recommendations from the datasheet.

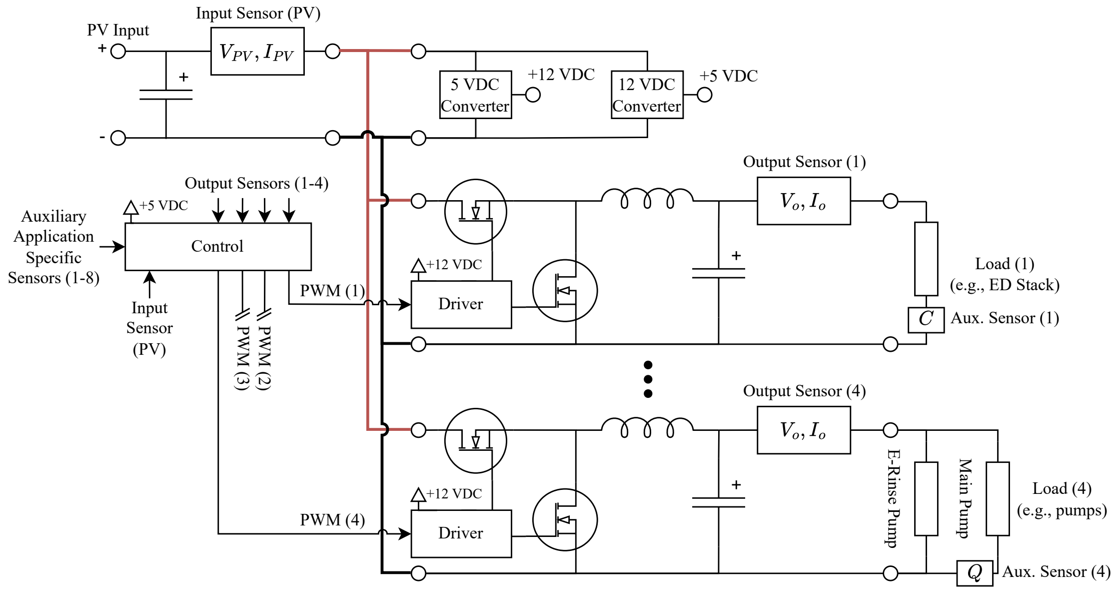

FIGURE 5. Hardware schematic and overall control structure of a multi-converter direct-drive system. Load (2) and Load (3), the extra buck converters are not directly shown and instead represented as an ellipsis to conserve figure space.

$$\Delta i/2 \leq < i_L > \quad (1)$$

2) Inductor Sizing

We used the canonical inductor voltage-current equation (2) with some approximations to estimate the minimum inductor size.

$$V = L * \frac{\mathrm{d}i}{\mathrm{d}t} \quad (2)$$

The first approximation is that di is the allowable current ripple, Δi, associated with the differential time period, dt, when the MOSFETs are in one state or another (e.g., state one: top MOSFET closed, bottom MOSFET open, and state two: top FET open, bottom MOSFET closed) related to the duty cycle, D, and period, T, defined as either DT, or $(1-D)T$. Substituting Δi for $2* < i_L >$ and considering the transient when the top switch is open and the bottom switch is closed, isolating the inductor, allowed us to reach Equation 3.

$$L \geq V_L * \Delta t/2* < i_o >= V_o * (1-D) * T/2* < i_o > \quad (3)$$

During the minimum operating current (worst-case) scenario, the current $< i_o >=< i_L >$ was calculated to be approximately 10 mA. If we consider the minimum possible duty to be 0 (s.t. $V_o = 60$), and a conservatively slow switching frequency of 10 kHz—relative to our microcontroller's (Teensy 4.1) processor speed, 600 MHz—we found our worst case inductance was approximately 0.3 H. In the case of maximum operating current (best-case), 2 A, the inductance needed to be 1.5 mH.

The worst-case scenario inductance was relatively high, and due to availability and cost, we decided to relax the current ripple constraint and utilized a 1.124 mH inductor (Wurth Elektronik 744139). Having higher current ripple at the low operating end may cause some periodic water dissociation; however, this periodic behavior was acceptable for our experimentation, as we were aiming to prove the validity of the design and control scheme, and periodic overlimiting behavior is sometimes employed in practical industrial operation. We also had the option of operating at higher switching frequencies, making the smaller inductance suitable for the current ripple requirement.

3) Capacitor Sizing

We then estimated the capacitance required (Eqn. 4), given the current ripple projected from the design (480 mA), our operating frequency (10 kHz, conservatively), and voltage ripple requirement (100 mV).

$$C \geq (1/8) * \Delta i * (T/\Delta V) \quad (4)$$

In our case, we found that we needed only 60 μF of capacitance. We ultimately chose an oversized capacitance of 2000 μF for both buck converters due to ease of component accessibility (two Panasonic ECA-2AM102). With these values, we expected a worst case current and voltage ripple of 480 mA and 3 mV, respectively.

4) Control Circuitry Design

The power for the control circuitry required a constant 5V rail and constant 12V rail. We selected two point of load (POL) power converters (Traco Power TSR 1-48120WI for the 12 V, and TSR 1-4850WI for the 5 V); we placed two of each converter in parallel to satisfy the current requirement of the control circuitry. Both the 5 V and 12 V rails had their outputs buffered with two parallel 1000 μF capacitors (KEMET ESK108M025AH4AA).

The high voltage PV input rail was buffered with four parallel 100 V, 1000 μF capacitors (Cornell Dubilier SLPX102M100A3P3) to aid in smoothing input PV transients.

We additionally included a relay (Omron G2RL-24 DC5) on one of the output converters, in case we wanted to do polarity reversal on the ED stack.

5) Sensing

The implemented sensors for the control algorithm consisted of the PV current and voltage sensor (Texas Instruments INA237AIDGST were used for all voltage and current measurements) for the MPPT algorithm, of the stack converter output current sensor for the feedback loop on limiting current, and the flow (Dijiang YF-S201) and conductivity sensor (Keyestudio KS0429) to calculate the limiting current. The flow rate was determined by reading the output pulse frequency from the flow meter and multiplying a calibrated value. Beyond these, we included voltage and current sensors on the outputs of all of the converters to observe the consumed pumping power.

Parameter	Value
Buck Converter Inductor (mH)	1.124
PV-side Capacitance (μF)	4000
Load-side Capacitance (μF)	2000
Switching Frequency (kHz)	10

TABLE 2. Parameters of the multi-buck converter system

A detailed block diagram for the board can be found in Appendix D.

C. SOFTWARE

The prototype MPPT and optimal desalination controller was implemented digitally on a microcontroller (Teensy 4.1).

Our control was run at the maximum rate the microcontroller could handle with our computation time. We output sensor data over USB serial to a computer using a script (Python) every 10 cycles. An average of 27 ms was seen between readings within the loop, indicating that the loop was running at approximately 2.7 ms per cycle.

In every loop, we checked to ensure the commanded duty cycle was not excessively high (>90%) as well as checked for undervoltage protection (<17 VDC) on the PV input; The 12 VDC POL converters, which supply our drivers, were not rated to operate below 17 VDC. We had additional low voltage shutoff conditions if the duty commanded was excessively low (<5%).

In each loop, we additionally read the current and voltage sensors over I2C, with readings internally averaged by the integrated chip 32 times. The output current and voltage sensors were read every 8 cycles, and the input current and voltage sensors were read every other cycle.

1) MPPT Algorithm

Every 4000 loop checks, we ran our MPPT algorithm, which led to an adjusted input voltage setpoint and a corresponding downstream alteration of voltage commanded to the loads. We heuristically found this to be a stable time period between MPPT algorithm checks; if we operated too quickly, the MPPT could become unstable because the input voltage tracking PID loop may not reach and settle at the MPPT setpoint quickly enough. This operation was conservatively slow, but still had the ability to prove our control scheme—which combines the MPPT operation with independent goals of downstream converters—is possible.

Our maximum PV voltage tracking setpoint was 26 VDC, to ensure we did not exceed the pumps' maximum rated voltages (24 VDC). The minimum PV voltage tracking setpoint was 18 VDC. We adjusted the algorithm in increments of 0.5 V due to current sensor noise; we needed a large enough change in overall power, above the noise floor, such that the MPPT can properly interpret the impact of its changes. We implemented a simple perturb and observe algorithm, as discussed earlier in Fig. 11. Input voltage and current sensors were averaged over 1000 readings, to aid with stability and noise.

We utilized a PID feedback loop with 8-bit resolution to alter the overall duty signal (D_1 in Fig. 4) to track the input voltage and match it to our voltage setpoint, set by the MPPT. This value is initialized as 18 VDC (just above the minimum operating voltage). The PID coefficients were: $K_p = 10, K_i = 1, K_d = 0$.

Square waves with differing duty cycles were created and digitally driven using interrupts to ensure consistency at a frequency of 10 kHz. We implemented a dead time fraction of 10% of the total period, approximately 10 μS.

2) Optimal Desalination Algorithm

Every cycle we read the flow and conductivity sensors. These readings were averaged over 100 readings to eliminate noise for the limiting current calculation. The flow meter was read using frequency (analog input translated to digital pulses if above and below a threshold) and the conductivity sensor was read with a linearly scaling analog input. The limiting current calculation was accomplished using a simple model [11] involving the multiplication of empirical fitting coefficients and the read flow and conductivity values. These coefficients are commonly empirically determined for different electrodialysis stacks. For the stack utilized (PC Cell, 20 cell pairs), these coefficients were determined to be $A = 1e - 5$ and $B = 0.4$. More details can be found in Appendix C.

The current commanded to the stack had its own dedicated PID loop to bias the duty cycle from the MPPT, D_1, by a weighting factor which was limited to a range, $0 < \alpha \leq 2$. The range was heuristic, and physically meant that the electrodialysis stack duty could be no more than two times the

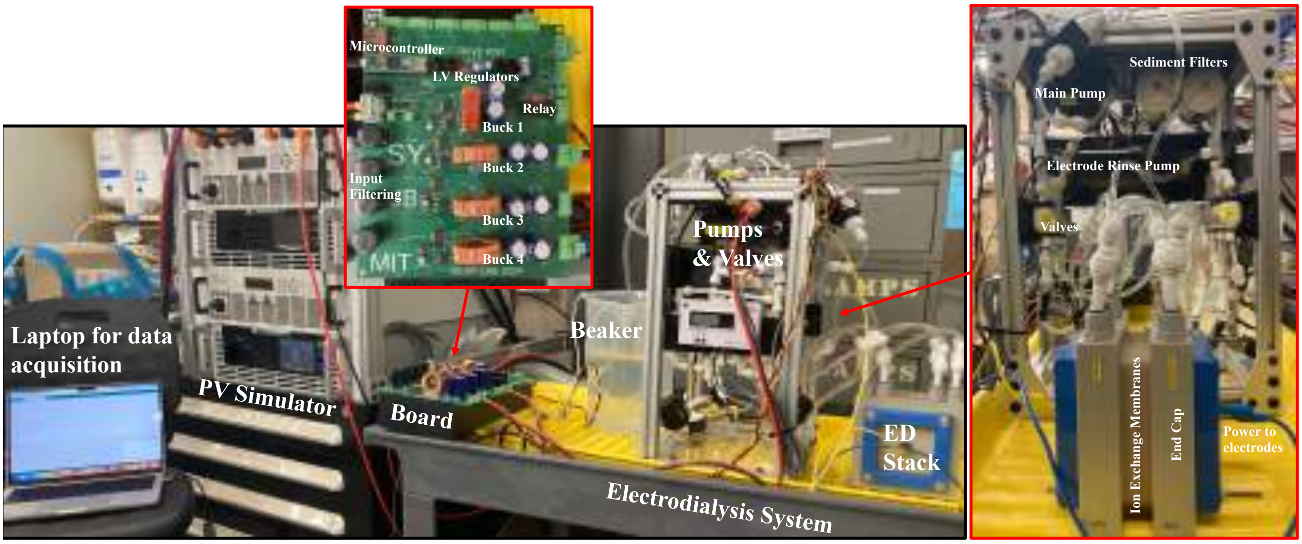

FIGURE 6. Labeled photograph of the experimental system setup, including details of the PCB and of the electrodialysis system.

duty commanded to the pumps' converter. The PID coefficients were: $K_p = 100, K_i = 100, K_d = 0$.

D. EXPERIMENTATION

1) Experimental hardware setup

The board was connected to a hydraulic rig (Fig. 6). The electrodialysis system was configured and operated in continuous mode, with one input feed stream and two output streams. The desalinated output water (diluate) and concentrated (brine) waste water were both sent to the feed water beaker (storage tank) in the end, allowing them to mix, return to their original concentration, and be reused as feed water. Water was transported from the beaker via the main pump and electrode rinse pump through sediment filters, valves, and then into the electrodialysis stack. The electrodialysis stack we utilized was a PC Cell 64002 with 20 cell pairs. After passing through the electrodialysis stack, the desalinated water and waste water exited via output valves into separate streams that were remixed into the feed water tank. Flow rate and conductivity were monitored immediately after the output valves. Additional analog manometers and digital conductivity sensors were placed immediately before and after the stack on both the product and brine streams, however, data from these were not required or recorded; they served as redundant sensing for troubleshooting during construction. The combined hydraulic layout is detailed in a block diagram in Fig. 7.

2) Experimental design

We conducted a series of tests with three replicates, using a combined power supply / solar simulator (Chroma 62120D-1200) to mimic the procedure detailed in EN 50530:2010 Sequence A, which examines the overall efficiency of grid connected photovoltaic inverters by stepping between a minimum and a maximum power available several times. The test is typically conducted with a ramp and has a controlled

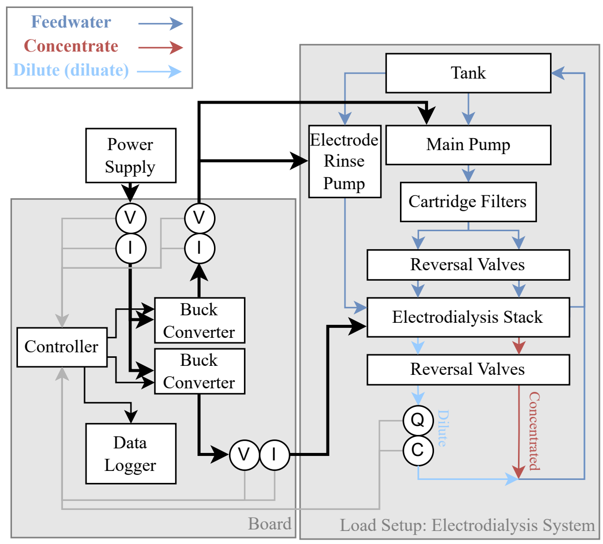

FIGURE 7. Experimental block diagram which includes the interfaces between the electronics and hydraulic architectures. Power flows are indicated in bold arrows. Sensing traces are denoted in gray. The sensors include voltage (*V*), current (*I*), conductivity (*C*), and flow rate (*Q*).

amount of time between ramps up and down. In our case, we unfortunately did not have access to the software to do this test exactly on the power supply; however, we were able to operate in a constant solar panel simulator environment and directly set the voltage maximum power point (V_{MP}), the maximum power output (P_{MP}), and the irradiance (IRR) to generate equivalent open circuit voltage (EQ_{VOC}), equivalent maximum power voltage (EQ_{VMP}), equivalent short circuit current (EQ_{ISC}), and equivalent maximum power current (EQ_{IMP}). We conducted a series of successive step responses in roughly

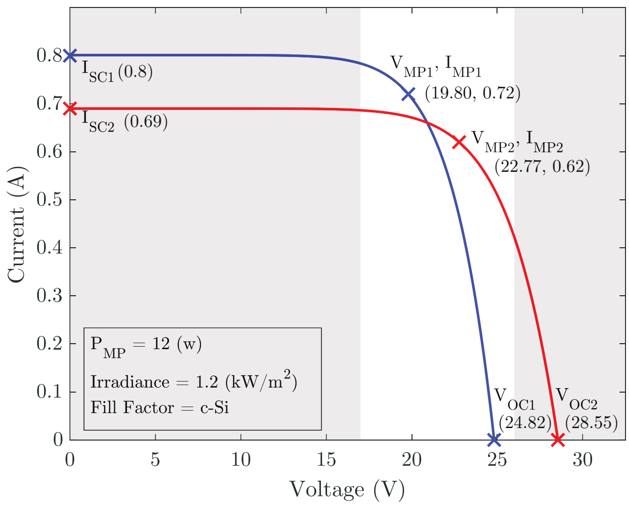

FIGURE 8. Characteristic solar panel current-voltage curves for the two different maximum power points (V_{MP1}, I_{MP1} and V_{MP2}, I_{MP2}) used in experimental validation. The shaded areas indicate regions outside of the system operating window. The lower bound operating voltage is constrained by the POL converters' minimum input voltage from the solar array (17 VDC). The upper bound voltage is constrained by a maximum operating voltage set in software (26 VDC). This voltage is set so that we operate under the maximum voltage of the pumps (24 VDC) when at maximum duty (0.9).

two minute intervals (manually, with a timer) between the two simulated solar panel profiles shown in Figure 8.

The physical intuition in lowering available voltage and increasing available current (and vise versa) on the solar simulator is related to the case of a solar panel undergoing reduced irradiance (lowering the short circuit current) and reduced temperature (increasing the open circuit voltage); this for instance could occur as a cloud passes over the panel, or as the sun sets. Characteristic IV curves are further discussed in Appendix A.

Our experimental bench-scale hardware limited the power bandwidth (see shaded region of Figure 8). The low setpoint point was a sufficient voltage to operate the POL converters and operate the pumps (Singflo 2401) and stack. The high setpoint was not set excessively high to avoid saturating the buck converters' duty cycle. The highest operating power was limited by the power consumption of the two pumps in parallel (24 VDC, 1A for each pump) and by the stack's limiting current. Our limitations in conductivity sensor range (1000 ppm maximum) constrained the limiting current (and thus applied current) to the ED stack, and the stack power was thus small relative to the pumps. The small stack area relative to industrial-scale applications also constrained the overall current applied.

Observing the overall system power and confirming its convergence to the maximum power point allowed us to confirm the functionality of the MPPT. Specifically, validating that the algorithm commands a voltage setpoint close to the maximum power voltage setpoint and that the controller draws the maximum current at that setpoint, ensures the MPPT is drawing the maximum power from the simulated solar array. Observing the commanded electrodialysis stack current and confirming its convergence to the limiting current allowed us to validate that the system was operating at the optimal desalination point. Accomplishing both of these objectives simultaneously validated the feasibility of the proposed multi-converter MPPT hardware and control scheme.

IV. RESULTS

A. MPPT TRACKING PERFORMANCE

Step responses of the multi-converter MPPT on the lab-scale electrodialysis system are shown in Figure 9. The response of voltage over the experiment is shown in Figure 9A, where the maximum power point voltage, V_{MP}, is stepped up and down, simulating EN 50530:2010 Sequence A. The multi-converter MPPT algorithm is shown altering the setpoint, $V_{setpoint}$ to track the maximum power point. The overall system voltage drawn, V_{PV}, is shown responding as the downstream converters accordingly adjust to track the setpoint, $V_{Setpoint}$. The MPPT algorithm is able to identify the voltage at the maximum power point, shown by the controller voltage setpoint, $V_{Setpoint}$, eventually identifying and tracking the maximum power point voltage, V_{MP}. The actual commanded voltage tracks the maximum voltage setpoint to a mean absolute percentage error (MAPE) of $4.1 \pm 0.5\%$. In summary, $V_{Setpoint}$ is properly, algorithmically tracking V_{MP}, and the actual simulated solar panel voltage, V_{PV} is tracking the desired control setpoint, $V_{Setpoint}$.

The behavior of simulated solar panel currents are shown in Figure 9B. The maximum available current, I_{MP}, shifts up and down converse to the voltage to maintain the constant overall power level (Fig. 8). The actual current drawn from the simulated PV panel by the entire system, I_{PV}, responds by approaching and similarly tracking the maximum available current. The actual commanded current tracks the maximum current setpoint to a mean absolute percentage error (MAPE) of $14.1 \pm 3.0\%$.

The convergence of V_{PV} to V_{MP} (Fig. 9A) and convergence of I_{PV} to I_{MP} (Fig. 9B) indicate the overall system is tracking the maximum available power and thus the maximum power point tracker portion of the controller is functioning as intended. The algorithm was relatively slow to find the maximum power point, in contrast to commercial MPPTs, but this was because we aimed for stability within our lower-level, individual converter control loops and did not aim for maximizing speed. We used conservative loop gains, were limited in bandwidth and speed by our actuators, and were limited in resolution and signal-to-noise ratio by the lower-cost sensors we utilized. Furthermore, we applied relatively large increments in $V_{setpoint}$ that resulted in hysteresis about the maximum power point; this hysteresis can be seen in the oscillations of V_{PV} about the maximum power point, $V_M P$ in Figure 9A. Lastly, the loop speed at which we adjusted the maximum power point, $V_{setpoint}$, was also limited in speed due to the need to wait for the internal, cascaded feedback controllers to respond to a new setpoint at a faster internal

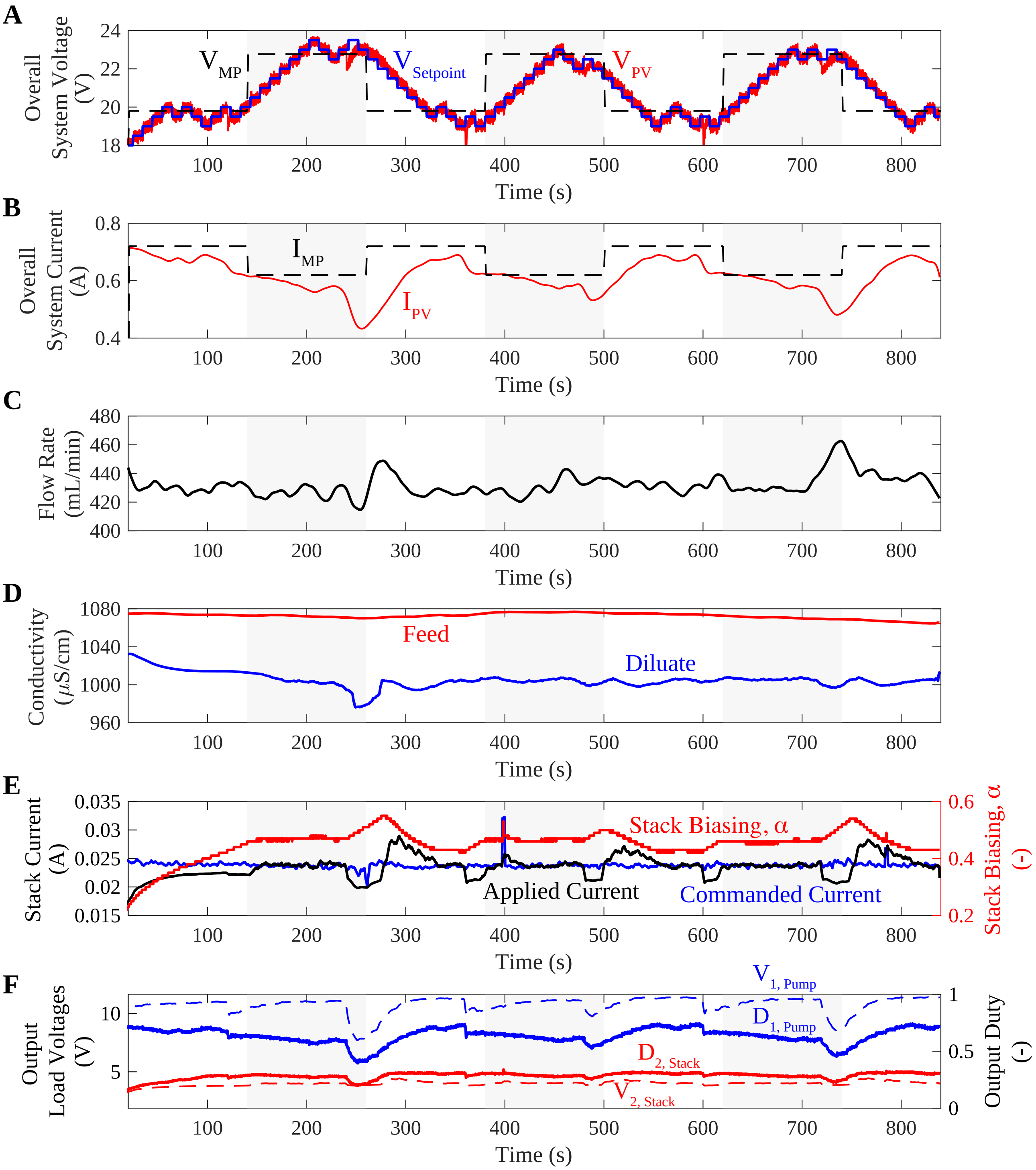

FIGURE 9. **(A) Step responses of the multi-converter MPPT on the lab-scale electrodialysis system, including the response of voltage over the experiment, where the maximum power point voltage, V_{MP}, is stepped up and down. The multi-converter MPPT algorithm alters the setpoint, $V_{setpoint}$ to track the maximum power point. The downstream converts adjust accordingly to draw an overall voltage, V_{PV}. Maximum available current, I_{MP}, in (B) is stepped up and down opposite voltage to maintain a constant power and the response of the actual overall current draw, I_{PV}, from the simulated solar panel is shown. The electrodialysis system flow rate (C) and conductivities (D) are shown throughout the experiment. (E) shows the empirically measured stack current, stack current command, and stack biasing coefficient. (F) presents the output voltage responses of each converter as solid lines, and the corresponding duty cycles as dashed lines, for the pump and stack loads. Shaded regions are included to distinguish between the steps up in voltage (and down in current) for ease of visual comparison across parameters measured.**

loop speed. In practice on a full-scale system, increasing the control loop sampling frequencies, optimizing the controller

TABLE 3. Tracking Error Summary

	Maximum Power Point			Max Desal. Rate
Error Metric	Voltage (V) $f(V_{MP}, V_{PV})$	Current (A) $f(I_{MP}, I_{PV})$	Power (W) $f(P_{MP}, P_{PV})$	Current (A) $f(I_{lim}, I_{stack})$
MAE	0.86 ± 0.11	0.08 ± 0.01	1.7 ± 0.2	0.0022 ± 0.0001
RMSE	1.2 ± 0.2	0.13 ± 0.01	2.6 ± 0.2	0.0032 ± 0.0001
MAPE	$4.1 \pm 0.5\%$	$14.1 \pm 3.0\%$	$14.3 \pm 2.3\%$	$10.3 \pm 0.3\%$

MAE = Mean Absolute Error, RMSE = Root Mean Squared Error, MAPE = Mean Absolute Percentage Error, where the error is calculated from the inputs as a function of the optimum and measured values: $f(optimum, measured)$. Error from $n = 3$ trials reported with standard deviation.

gains, and choosing alternative actuators would improve the maximum power point tracking and response speed.

A full summary of tracking errors over the trials can be found in Table 3.

B. INDEPENDENT LOAD REGULATION

Figure 9C shows the flow rate of the system during the experiment. The flow rate plotted was smoothed with a moving average with a span of 1000 samples. The flow rate remains roughly the same throughout experiment, with perturbations during maximum power point step changes. We only track the diluate flow rate, but with the channels being equal in hydraulic resistance, the concentrate stream should be approximately the same flow rate. The flow rate informs the limiting current of the electrodialysis system.

Figure 9D shows the conductivity of the feedwater stream and diluate water stream. The feed remains relatively constant and the diluate does not continue to decrease over time because of the brine and diluate streams remixing to reconstitute the feed and the continuous operation of the system. The concentrations were expected to remain constant with the exception of responses to any perturbations during maximum power point tracking. The diluate output conductivity fluctuations are closely related to the flow rate and current applied. The greater the applied current, the proportionally lower the output conductivity. Slower flow rates create longer residence times within the stack, which also lower output conductivity. Because the flow rate and applied electrodialysis stack current were relatively stable throughout the experiment, the fluctuations in diluate conductivity were not dramatic.

The diluate conductivity and flow rate influence the limiting current and thus the commanded current to the electrodialysis stack in Figure 9E. This commanded current was roughly constant throughout the experiment because the flow rate and diluate conductivity were also relatively constant. There are the exception of a few perturbations influenced by the initial drop in diluate conductivity and a separate brief spike around 400 seconds likely due to sensor noise. The current command setpoint was achieved by altering the stack biasing factor, α, which in turn affected the stack power converter's duty cycle. The stack biasing factor fluctuated in response to MPPT voltage setpoint changes. The applied current correspondingly matches the commanded current once settled, despite the fluctuations in the input voltage for the ED stack converter. The applied current, (i_{stack}), tracks the optimal current (i_{lim}) with a MAPE of $10.3 \pm 0.3\%$ over the entire experiment of perturbations. This indicates that this downstream converter is able to accomplish its individual objective, maximizing and tracking limiting current, while simultaneously adapting to maximum power point changes.

Lastly, the duty cycle signals for both of the converters and their output voltages can be seen in Figure 9F. The duty cycles, D_{pump}, D_{stack}, directly affected the voltages on the pump, V_{pump}, and stack, V_{stack}, and were changing in response to the alterations in V_{MP}. Perturbations in the maximum power point consistently initially dropped the duty commanded for both the pump and stack, before the duty increases appropriately and the optimal voltages were commanded. The independent duty cycles show that the two downstream converters have independent load control, while still tracking the maximum power point.

These results demonstrated that the simultaneous tracking of the maximum power and the optimal allocation of power to independent, downstream loads is feasible using the proposed control scheme and architecture.

V. DISCUSSION

Practically, by embedding MPPT directly into the control logic of multiple downstream converters, this approach eliminates the need for both an upstream DC/DC converter, which is often used as a centralized MPPT stage, as well as eliminates the need for battery storage. In conventional off-grid systems, a dedicated MPPT DC/DC converter and energy storage can represent a substantial portion of system cost. Eliminating this hardware not only reduces capital expenditure and system complexity, but also improves reliability by removing a critical point of failure. This contributes to a simpler, more resilient architecture, ideal for remote or resource-constrained environments.

However, our results were constrained by several hardware limitations. The low-cost sensors used for flow rate, conductivity, and current introduced signal noise, reduced dynamic response, and restricted operation to low salinities. These limitations, along with the narrow voltage range of the pump and the brackish-range conductivity sensor, resulted in the pumping energy being a much higher proportion of overall energy consumption than would typically be expected in larger-scale or seawater-based implementations. In practice, ED stacks operating at higher salinities often consume power at levels comparable to or even exceeding those of pumps. Our constrained power bandwidth also precluded outdoor testing with real solar panels, as the system would have quickly saturated under higher irradiance, limiting the ability to evaluate dynamic MPPT performance throughout the day.

Future work should explore higher-performance hardware, including variable frequency drives (VFDs), high-dynamic-range sensors, and broader power range actuators. Testing the algorithm with seawater salinity feeds, higher current densities, and scaled-up stacks would provide more realistic insights into system-level tradeoffs. Additionally, incorporating multiple ED stacks or entirely different loads—such as temperature-differentiated refrigeration units—would allow exploration of power distribution strategies across varied electrochemical or thermal applications. Alternative control algorithms beyond traditional feedback loops may also yield improved performance in more complex applications.

Overall, this work presents a foundational step toward fully eliminating energy storage in renewable-powered desalination and other electrochemical processes. While this study focused on desalination, the underlying control strategy is closely applicable to other solar-powered electrochemical systems, such as carbon dioxide electroreduction, electrolysis for chemical synthesis or hydrogen production, wastewater electro-oxidation, and electrowinning, where maximizing throughput under variable solar input is essential. This work provides a practical control strategy for direct-drive, multi-objective solar systems, offering a path toward higher efficiency, lower cost, and more sustainable off-grid infrastructure.

VI. CONCLUSIONS

This work demonstrates a novel architecture and control strategy for direct-drive photovoltaic (PV) systems supplying multiple independent loads without energy storage. We developed and experimentally validated a multi-converter maximum power point tracker (MPPT) that dynamically allocates power between an electrodialysis (ED) desalination stack and a hydraulic subsystem. Our nested feedback control algorithm adjusts power allocation using a continuously updated biasing factor on the ED stack converter's duty cycle. Using a lab-scale prototype, we achieved real-time maximum power point tracking while independently regulating load behavior; the system maintained operation at the ED stack's limiting current while tracking the PV module's maximum power point, demonstrating optimal desalination throughput and solar utilization without any form of energy storage or buffering. This is a step toward simple, low-cost, solar-powered water treatment.

APPENDIX A
CHARACTERISTICS OF PHOTOVOLTAIC PANEL IV CURVES

Photovoltaic panels have current-voltage (IV) curves which are characterized by a relatively constant short-circuit panel current which drops rapidly close to the open circuit panel voltage (Fig. 10). As solar irradiance increases during the day, the incident sunlight increases the amount of available current; however, the panel remains voltage limited by its open circuit panel voltage. Even early on in the day, with limited sunlight, the panel will reach its open circuit voltage quickly - but will be limited in that very little current can be drawn before rapidly dropping the panel voltage.

Aside from the variations in IV curves due to irradiance, there are variations in panel behavior due to temperature. Decreasing the temperature of the photovoltaic array will increase the open circuit voltage, and thus the power available for a panel of equivalent available current. Conversely, increasing the temperature increases losses via resistance in the system and in the crystal lattice of the doped silicon. This is why many panels on larger or more complex arrays may be actively or passively cooled [18].

Additionally, the solar panel array configuration affects the characteristic IV curve seen downstream of the system. An array in series increases the open circuit voltage, but does not effect the short circuit current. An array in parallel increases the short circuit current, but does not increase the open circuit voltage. This translates to a shifting of the IV curve upward (parallel) or to the right (series).

Other effects which affect IV curves include mismatch losses such as partial shading of solar arrays, soiling of the array, and damaged cells. These are particularly challenging, in that they create multiple local optima for maximum power [19]. Additional characteristic features of the IV curve for a PV panel are caused by series and shunt resistances. Series resistances will decrease the trailing edge slope, and shunt resistances will increase the leading edge slope.

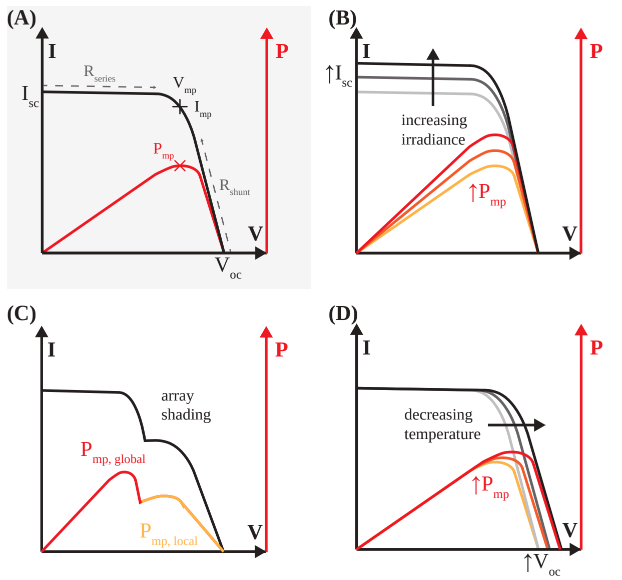

FIGURE 10. Conceptual Characteristic Current-Voltage (IV) Curves for a solar panel, not drawn to scale, where A) demonstrates a canonical IV curve for a photovoltaic panel including V_{mp}, I_{mp}, the voltage and current at which maximum power, P_{mp} exists. I_{sc} and V_{oc} are the operational extremes of short circuit current and open circuit voltage, respectively. R_{series} and R_{shunt} are the parasitic series and shunt resistances within the photovoltaic panel which characterize the leading and trailing edge IV curve slopes, respectively. B) demonstrates the increasing I_{sc} with irradiance, C) shows the effects of array shading on the IV curve and multimodal power curve, and D) shows the increasing shift of V_{oc} with decreasing temperature.

APPENDIX B
MAXIMUM POWER POINT TRACKERS

Maximum power point trackers are algorithms that can pull the maximum power from a solar array despite intermittencies and variations due to the aforementioned factors altering the characteristic IV curves. They function by algorithmically determining the optimal amount of voltage and current to draw from the PV panel. MPPTs are often coupled with a power converter, which converts the photovoltaic panel voltage to an applied load, often a battery in off-grid scenarios. The output voltage of this converter to the battery is relatively constant and steady, while the input voltage from the photovoltaic panel can vary depending on the current drawn from the panel. This current varies based on the duty cycle to switches in the converter, which are often metal oxide field effect transistors (MOSFETs) or insulated-gate bipolar transistors (IGBTs), though alternatives are under research and development (e.g., GaN [20]).

A wide gamut of MPPT algorithms exist; however, two common and conceptually simple algorithms include fractional open circuit voltage (FOCV) and perturb & observe (P&O). FOCV is a conventional, indirect method that measures only the panel voltage. It aims to keep the panel voltage at a fixed fraction of the known, open circuit voltage. This method is quite simple and highly robust, but fails to track the maximum power point - especially with changes in temperature or shading. FOCV can be implemented with a simple feedback loop with reference on the target fractional panel voltage and process variable on the measured panel voltage. P&O is another common technique which is a hill-climbing method (Fig. 11). It iteratively compares the power to the previous timestep to see if there is an increase or decrease, and then compares the voltage to the previous timestep to determine the direction in which the algorithm had been traveling. It takes these two factors into a simple decision tree and then incrementally changes the duty cycle directly on the power converter (or can alternatively change the reference voltage, which is fed back into a FOCV algorithm).

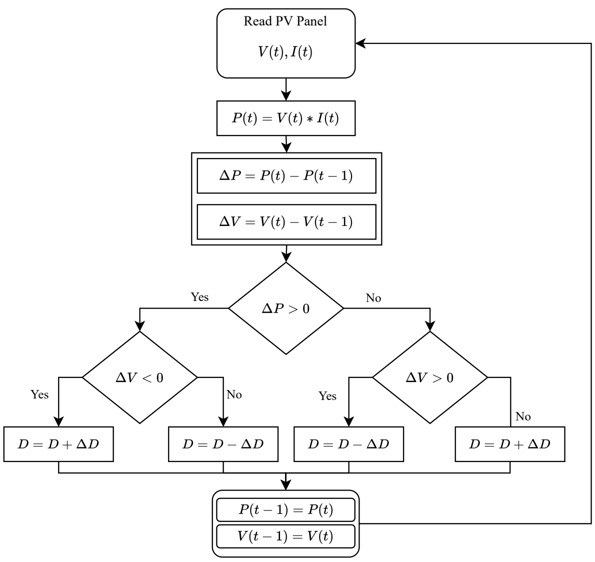

FIGURE 11. **Flowchart of an example MPPT algorithm: perturb and observe, also known as a hill climbing method. Where, $V(t)$, $I(t)$ represent the sensed panel voltage and current, respectively, and $P(t)$ represents the panel power at time t. The change in power, ´P and change in voltage, ´V at each iteration is used to determine the increase or decrease in duty, D by a preset increment, ´D. Though, algorithms may exist which can adaptively change this duty cycle.**

Generally, MPPT algorithms can measure voltage, current, solar irradiance the panel array temperature, as well as in more complicated cases make weather predictions, and discretize these measurements into pieces of a broader array. Many more complex MPPT algorithms have been proposed [21].

APPENDIX C
LIMITING CURRENT FITTING

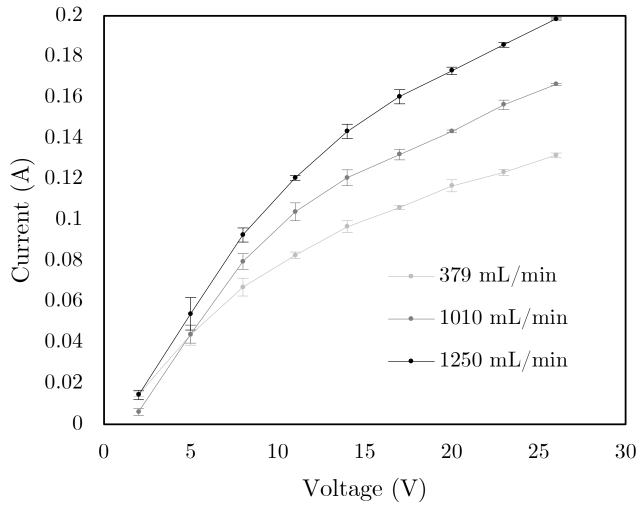

FIGURE 12. **Current-voltage curve for the electrodialysis stack, consisting of the ohmic and limiting regions. Where in the ohmic region at relatively low voltages, the current increases linearly. In the limiting region, the current increases at a decreased rate with increases in voltage. Three curves are shown at different water flow rates of 379, 1010, and 1250 mL/min, corresponding to pump voltages of 6.4, 10, and 14.4 VDC, respectively. The diluate concentration measured for each of these readings was 690 +/- 107 mg/L from a feedwater of 922 +/- 2.8 mg/L. Reported values are the average, with standard deviation as the measurement of error.**

To operate at the optimal (fastest) desalination rate in direct-drive electrodialysis [13], the system must operate at or near the constraint of limiting current. The limiting current occurs when the boundary layer adjacent to the membrane is completely depleted of solute; at this point, any excess voltage begins to cause some dissociation of the water molecules [22].

The limiting current varies nonlinearly with both the concentration of the solution in the diluate compartment and the water flow velocity. This nonlinear relationship is often determined empirically, by examining current-voltage curves (CVCs). The membranes, spacer geometry, materials, number of cell pairs, and water composition all also affect the CVC behavior, which is why limiting current models are almost always empirically derived.

In the CVC, the transition between the ohmic and limiting region is traditionally marked as the limiting voltage and current for the given concentration and flow rate. Examining several of these points can allow the empirical fit of several different models which describe the limiting current at different concentration and flow rates. For this work, we utilize the Equation 5.

$$i_{lim} = \alpha * C * Q^{\beta} \quad (5)$$

Where α and β are fit coefficients, C is the concentration of the solution in mg/L, and Q is the flow rate in mL/min. The units of concentration and flow rate for the fitting are arbitrary, so long as they are consistent with the sensor readings in practice.

Figure 12 shows the CVC for our electrodialysis stack. In this case, we determine the limiting voltage to exist roughly at 11 VDC for all of curves, but with varying limiting currents of 0.08, 0.10, and 0.12 A for each of the flow rates in increasing order. Using a numerical solver, we identify fitting constants of $\alpha = 1e-5$ and $\beta = 0.4$, for our setup. This limiting current equation was utilized within the "Electrodialysis Limiting Current Model" block shown in Figure 4.

APPENDIX D
DUAL BUCK MPPT CONVERTER BLOCK DIAGRAM

Figure 13 shows a block diagram of the components utilized in the experimental prototype. The input PV voltage bus feeds several downstream converters. These consist of constant voltage converters for the drivers, controllers, and sensors as well as the higher power converters that drive the dominant actuators: the pump and electrodialysis stack. The controller sends pulse width modulated (PWM) signals to the respective buck converter, which consists of a FET driver and lowpass output LC filter. Several general purpose sensor inputs were made available for voltage sensing to accomodate the low-cost sensors; however, some drawbacks include that these were susceptible to noise (in contrast to current sensing).

ACKNOWLEDGMENT

J. T.-Y. B. would like to thank S. Leeb for his feedback and J. Costello for his enthusiasm.

REFERENCES

[1] F. Creutzig, P. Agoston, J. C. Goldschmidt, G. Luderer, G. Nemet, and R. C. Pietzcker, "The underestimated potential of solar energy to mitigate climate change," *Nature Energy*, vol. 2, no. 9, pp. 1–9, 2017.

[2] K. Bharath *et al.*, "A novel sensorless hybrid mppt method based on focv measurement and p&o mppt technique for solar pv applications," in *2019 International Conference on Advances in Computing and Communication Engineering (ICACCE)*. IEEE, 2019, pp. 1–5.

[3] M. L. Katche, A. B. Makokha, S. O. Zachary, and M. S. Adaramola, "A comprehensive review of maximum power point tracking (mppt) techniques used in solar pv systems," *Energies*, vol. 16, no. 5, p. 2206, 2023.

[4] S. Jain, A. K. Thopukara, R. Karampuri, and V. Somasekhar, "A single-stage photovoltaic system for a dual-inverter-fed open-end winding induction motor drive for pumping applications," *IEEE Transactions on power Electronics*, vol. 30, no. 9, pp. 4809–4818, 2014.

[5] W. Wareesri and S. Po-Ngam, "A three-phase pv-pump inverter with maximum power point tracking (mppt) controller," in *2016 13th international conference on electrical engineering/electronics, computer, telecommunications and information technology (ECTI-CON)*. IEEE, 2016, pp. 1–4.

[6] N. P. Korlepara, E. Elanchezhian, S. Pragaspathy, and S. Subramanian, "Novel multi-port converter for distributed mppt operation in solar pv system," *Science and Technology for Energy Transition*, vol. 79, p. 32, 2024.

[7] L. Gevorkov, J. L. Dominguez-Garcia, L. T. Romero, and A. F. Martinez, "Modern multiport converter technologies: A systematic review," *Applied Sciences*, vol. 13, no. 4, p. 2579, 2023.

[8] A. K. Bhattacharjee, N. Kutkut, and I. Batarseh, "Review of multiport converters for solar and energy storage integration," *IEEE Transactions on Power Electronics*, vol. 34, no. 2, pp. 1431–1445, 2018.

[9] S. Rahman, I. Khan, K. Rahman, S. Al Otaibi, H. I. Alkhammash, and A. Iqbal, "Scalable multiport converter structure for easy grid integration of alternate energy sources for generation of isolated voltage sources for mmc," *Electronics*, vol. 10, no. 15, p. 1779, 2021.

[10] C. Matus, H. Young, B. Pavez, P. Burgos, C. Cifuentes, and C. Lazcano, "Integration of renewable sources with multiport converter to supply electrolyzers," in *2024 IEEE International Conference on Automation/XXVI Congress of the Chilean Association of Automatic Control (ICA-ACCA)*. IEEE, 2024, pp. 1–5.

[11] H. Strathmann, "Electrodialysis, a mature technology with a multitude of new applications," *Desalination*, vol. 264, no. 3, pp. 268–288, 2010.

[12] W. He, A.-C. Le Henaff, S. Amrose, T. Buonassisi, I. M. Peters, and A. G. Winter, "Flexible batch electrodialysis for low-cost solar-powered brackish water desalination," *Nature Water*, vol. 2, no. 4, pp. 370–379, 2024.

[13] J. T.-Y. Bessette, S. R. Pratt, and A. G. Winter V, "Direct-drive photovoltaic electrodialysis via flow-commanded current control," *Nature Water*, pp. 1–9, 2024.

[14] K. G. Nayar, P. Sundararaman, J. D. Schacherl, C. L. O'Connor, M. L. Heath, M. Orozco Gabriel, N. C. Wright, and A. G. Winter, "Feasibility study of an electrodialysis system for in-home water desalination and purification in urban india," in *International Design Engineering Technical Conferences and Computers and Information in Engineering Conference*, vol. 57076. American Society of Mechanical Engineers, 2015, p. V02AT03A046.

[15] S. R. Shah, N. C. Wright, P. A. Nepsky *et al.*, "Cost-optimal design of a batch electrodialysis system for domestic desalination of brackish groundwater," *Desalination*, vol. 443, pp. 198–211, 2018.

[16] S. R. Shah, S. L. Walter *et al.*, "Using feed-forward voltage-control to increase the ion removal rate during batch electrodialysis desalination of brackish water," *Desalination*, vol. 457, pp. 62–74, 2019.

[17] M. Floryan, Q. Bowers, Z. Sternberg, S. Gembali, A. Goyal, J. Bessette, S. Honarparvar, and A. Winter, "Lab-to-market design of an electrodialysis-based home-scale water desalination system," in *International Design Engineering Technical Conferences and Computers and Information in Engineering Conference*, vol. 87318. American Society of Mechanical Engineers, 2023, p. V03BT03A017.

[18] J. Siecker, K. Kusakana, and e. B. Numbi, "A review of solar photovoltaic systems cooling technologies," *Renewable and Sustainable Energy Reviews*, vol. 79, pp. 192–203, 2017.

[19] G. G. Kim, W. Lee, B. G. Bhang, J. H. Choi, and H.-K. Ahn, "Fault detection for photovoltaic systems using multivariate analysis with electrical and environmental variables," *IEEE Journal of Photovoltaics*, vol. 11, no. 1, pp. 202–212, 2020.

[20] E. A. Jones, F. F. Wang, and D. Costinett, "Review of commercial gan power devices and gan-based converter design challenges," *IEEE journal of emerging and selected topics in power electronics*, vol. 4, no. 3, pp. 707–719, 2016.

[21] A. Mohapatra, B. Nayak, P. Das, and K. B. Mohanty, "A review on mppt techniques of pv system under partial shading condition," *Renewable and Sustainable Energy Reviews*, vol. 80, pp. 854–867, 2017.

[22] M. La Cerva, L. Gurreri, M. Tedesco, A. Cipollina, M. Ciofalo, A. Tamburini, and G. Micale, "Determination of limiting current density and current efficiency in electrodialysis units," *Desalination*, vol. 445, pp. 138–148, 2018.

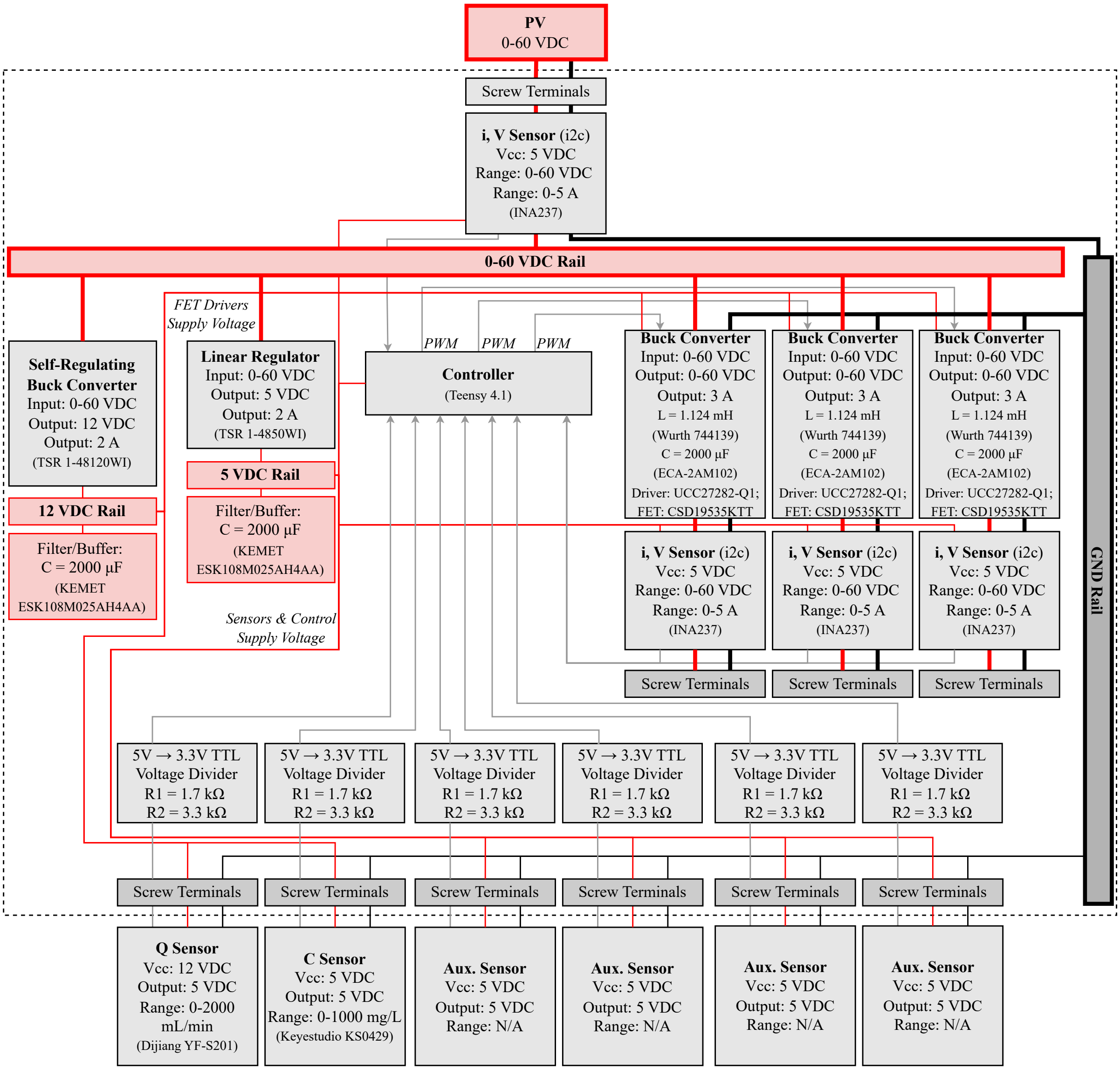

FIGURE 13. Dual Buck MPPT Converter Block Diagram.

JONATHAN T.-Y. BESSETTE is a PhD candidate within the K. Lisa Yang Global Engineering and Research (GEAR) Center at MIT. His research is focused on the development of desalination and water treatment systems for resource-constrained environments: from off-grid communities in India to oil & gas in the Permian. Bessette earned a BS from the SUNY University at Buffalo (2020) in mechanical engineering with a minor in studio art, and an MS (2022) from MIT in mechanical engineering. Bessette is a Fulbright scholar (2017), Marshall Scholar finalist (2020), and NSF GRFP recipient (2020). He received the International Desalination Association Innovation Award (2023) for his work, was a European Desalination Society Miriam Balaban Innovation Award Finalist (2023), was in the inaugural Morningside Academy for Design at MIT (2022), and was a J-WAFS Rasikbhai L. Meswani Fellow (2024). He has previously worked as a researcher at Stanford in radioglaciology, at Moog as an aircraft systems engineer, and as a mechanical engineer at Corning. He is also a volunteer EMT.

SHANE R. PRATT is a Staff Engineer at the K. Lisa Yang Global Engineering and Research (GEAR) Center at the Massachusetts Institute of Technology (MIT), where he leads the design and deployment of electromechanical and control systems for experimental research in water, energy, and agricultural technologies. He brings over a decade of hands-on experience in rapid prototyping, embedded systems, and field-deployable automation solutions. In addition to his role at MIT, Mr. Pratt is an independent engineering consultant specializing in early-stage hardware development. His portfolio includes solar panel cleaning robots deployed nationwide, mechatronic control systems for construction robotics, and electric propulsion systems for marine vessels. Previously, he contributed to hybrid drone R&D at Top Flight Technologies and led systems design at the MIT Auto-ID Lab. Originally from South Africa, Mr. Pratt combines a passion for engineering with a deep commitment to social and environmental impact. He is the co-founder and CTO of a startup advancing decentralized water treatment technologies powered by renewable energy, with applications across oil & gas, agriculture, and underserved communities. His work has been published in Nature Water, Applied Energy, and Engineering Applications of Artificial Intelligence. Mr. Pratt holds expertise in robotics, embedded programming, industrial controls, and IoT networks. He is dedicated to mentoring the next generation of engineers, particularly through hands-on teaching and open-access fabrication spaces.

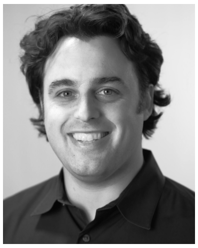

AMOS G. WINTER, V. is the Germeshausen Professor of Mechanical Engineering and the Director of the K. Lisa Yang Global Engineering and Research (GEAR) Center at MIT. His research focuses on machine and product design for developing and emerging markets. Prof. Winter earned a BS from Tufts University (2003) and an MS (2005) and PhD (2011) from MIT, all in mechanical engineering. He received the 2010 Tufts University Young Alumni Distinguished Achievement Award, the 2012 ASME/Pi Tau Sigma Gold Medal, was named one of the MIT Technology Review's 35 Innovators Under 35 (TR35) for 2013, and received the MIT Edgerton Faculty Achievement Award and an NSF CAREER award in 2017. Prof. Winter is the principal inventor of the Leveraged Freedom Chair (LFC) developing world wheelchair, which was a winner of a 2010 R&D 100 award, was named one of the Wall Street Journal's top innovations in 2011, received a Patents for Humanity award from the U.S. Patent and Trademark Office in 2015, and was the subject of "Engineering Reverse Innovations", winner of the 2015 McKinsey Award for the best article of the year in Harvard Business Review.